7.6 CLOUD CLIMATOLOGY OF THE SHEBA YEAR DERIVED FROM AN AUTOMATED ARCTIC CLOUD MASK

Douglas A. Spangenberg*, Venkatesan Chakrapani
Analytical Services & Materials, Inc., Hampton, Virginia

Patrick Minnis
NASA-Langley Research Center, Hampton, Virginia

1. INTRODUCTION

Determination of cloud radiation interactions over large areas of the Arctic is possible only with the use of data from polar orbiting satellites. Detecting clouds using satellite data over the Arctic is difficult due to the minimal contrast between clouds and the underlying snow surface in visible and infrared wavelengths. Polar clouds are frequently warmer or at the same brightness temperature as the background surface, complicating cloud detection. The frequent occurrence of some obscuring layer such as haze, diamond dust, or thin ground fog in the Arctic often makes it difficult to validate satellite cloud amounts. The use of the brightness temperature differences between the NOAA-AVHRR 3.7 and 11-µm channels (T3-4) aids the detection considerably during the day and at night. In strong daylight, the solar-reflected component of the 3.7-µm radiance provides a strong signal of the presence of clouds over snow. At night, the scattering of upwelling radiation from within the cloud at 3.7 µm enables the detection of low clouds using T3-4. However, at high solar zenith angles (SZA), the solar-reflected component at 3.7 µm is nearly cancelled by the internal scattering by the cloud resulting in a small apparent difference in T3-4 for clear and cloudy scenes.

In this study, an automated Arctic cloud mask is used to discriminate between clouds and the background snow surface over the Surface Heat Budget of the Arctic Ocean (SHEBA) ship site for daytime, nighttime, and twilight scenes between January 1998 and July 1998. The satellite-derived cloud amounts are validated by comparing them to cloud radar and lidar data within a 25-km radius surrounding the ship. Monthly-mean cloud amount, height, and cloud radiative forcing values are computed in the immediate vicinity of the SHEBA ship and over a larger domain in the western Arctic Ocean.

* *Corresponding author address:* Douglas A. Spangenberg, AS&M, Inc., Hampton, VA, 23666; e-mail: d.a.spangenberg@larc.nasa.gov

2. DATA

For this study, NOAA-12 and 14 AVHRR 1-km satellite orbits that encompass the SHEBA site and surrounding area are used. There is a total of 300-350 satellite orbits for any given month of 1998. The hours sampled by NOAA-12 and 14 include all except 20-24 local time (LT). The cloud mask was run at the 1-km pixel level with the resulting clear and cloudy pixels averaged onto a 25-km radius centered on the SHEBA site and over a 56x56km^2 regional grid. Figure 1 shows the ship track and regional analysis grid. European Center for Medium-Range Weather Forecasting (ECMWF) profiles were used in the cloud mask and cloud height algorithms.

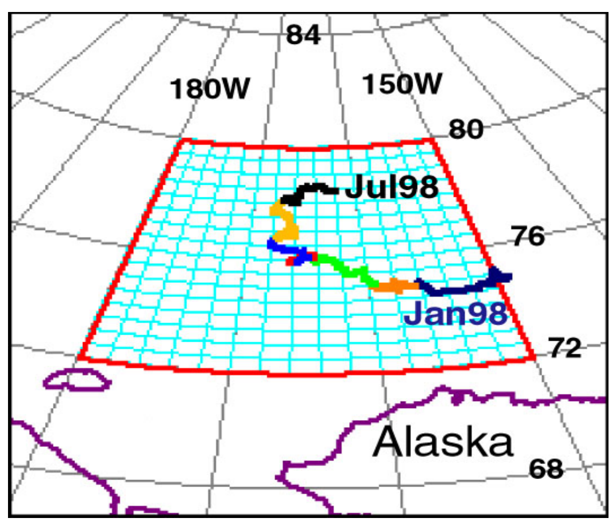

Figure 1. SHEBA ship track and analysis domain.

3. CLOUD MASK

Inputs to the automated Arctic cloud mask include NOAA-12 and 14 0.65 μm (R_{06}), 3.7 μm (T3), 11 μm (T4), and 12 μm (T5) channel data. ECMWF profiles were used in the correlated-k method of Kratz (1995) to obtain clear-sky background temperatures. To remove noise from the AVHRR 3.7-μm band at low temperatures, we used the parametric Wiener filter technique of Simpson and Yhann (1994). The filter works best at night when the T3 and T4 images have the same patterns.

For daytime hours defined as SZA > 82^o, the cloud mask uses theoretical 3.7-μm reflectance models over snow (Spangenberg et al., 2001), along with the Cloud's and the Earth's Radiant Energy System (CERES) polar mask framework developed for TERRA-MODIS (Trepte et al. 2001). The daytime mask compares the reflected part of the T3 radiance (R_{37}) with the clear-sky snow model value to discriminate clear-sky from snow-covered surfaces. The variability in clear-sky R_{37} was obtained from the subjective cloud mask of Minnis et al. (2001), which was run during the FIRE-ACE May-July 1998 intensive observation period. During the melt season, R_{06}, R_{37}, and T4 threshold tests are used to supplement the R_{37} snow model test. Detecting Arctic haze from otherwise clear pixels is accomplished by flagging high values of the brightness temperature difference between T4 and T5 (T4-5), generally above 0.7 K.

For nighttime (SZA > 90^o) and twilight (82^o < SZA < 90^o) scenes, cloud amounts are determined strictly from the brightness temperature threshold approach of Spangenberg et al. (2002). Much of the polar nocturnal clouds are picked up using the T3-4 test for low clouds having temperatures higher than the background snow surface. These clouds have relatively low T3-4 values. For twilight, the nighttime algorithm was modified to account for weak solar radiation hitting the tops of the clouds. Also, because of the relatively high R_{37} for forward scatter at high view angles, a special case of twilight tests is applied for this viewing geometry. Because of the difficulty in classifying pixels as clear or cloudy at night, weak clear and weak cloud categories are defined. The weak categories are likely to contain Arctic haze, thin cirrus, steam fog, or diamond dust.

4. VALIDATION

Satellite-derived cloud amounts from the polar mask are validated by comparing them with NOAA Environmental Technology Laboratory (ETL) millimeter-wave cloud radar (MMCR) cloud amounts. NOAA-ETL depolarization and backscatter unattended lidar (DABUL) was used to confirm the MMCR cloud amounts. If the radar and lidar disagreed, that particular satellite orbit time was excluded from the comparison. The satellite cloud amounts were computed by averaging all the cloud mask pixels falling in a 25-km radius centered on the SHEBA ship. MMCR cloud amounts are 20-minute time averages of cloud boundary data centered at the satellite overpass times. Table 1 shows the monthly-mean cloud amounts from the radar and automated cloud mask, including root-mean-squared (rms) errors between the two. Weak cloud or weak clear amounts over the SHEBA radius exceeding 10% were excluded from the validation. The best agreement between the cloud mask and radar occurred in July 1998, with an rms error of 17.6%. This is to be expected because it is easiest to detect clouds during perpetual daylight over dark melt ponds and open ocean surfaces. Highest rms errors occurred in April when abundant twilight is present along with very high SZAs. Also, the daytime algorithm misses some of the thin cirrus clouds over snow because there is little or no sign of them in the T3-4, T4-5, and T4 imagery. Satellite cloud amounts were underestimated in January and July by about 6%, while in April they were underestimated by about 15%. The ground-based cloud radar is tuned to see all types of thin clouds, while the satellite cloud detection threshold is somewhat lower, especially over cold snow surfaces.

Table 1. SHEBA monthly-mean cloud amounts and rms errors for the radar and satellite.

Month	Radar%	Sat%	RMS%	# Radii
January	65.1	58.8	24.8	116
April	94.5	79.1	32.3	220
July	98.2	91.8	17.6	99

5. RESULTS

Monthly-mean cloud amounts, heights, and TOA cloud forcing values were derived using the time and space averaging method of Young et al. (1998). The values were computed both over the regional grid (Fig. 1) and a 25-km radius surrounding the SHEBA site. The January-July 1998 cloud amounts are shown in Fig. 2. The cloud cover is a minimum in winter, with values near 40%. The values hold nearly steady from 70-80% for the spring and summer months. Cloud amounts are similar for SHEBA and the surrounding regional grid except for July, when the SHEBA site had 10% more cloud cover.

Cloud-top heights were computed by finding the lowest altitude in the ECMWF temperature soundings where T(z)=T4. The cloud height may therefore be underestimated with the case of thin clouds above a warmer surface. Figure 3 shows the cloud-top heights observed from January-July 1998. Regional grid values peak in February at 3.4 km with values around 2.7 km in the other months. This peak is likely due to the abundance of cirrus occurring during February. Cloud heights for the SHEBA ship are noticeably higher in July than for the regional grid, with heights peaking out at 3.5 km. This maximum in cloud height is probably resulting from stronger storm systems associated with the water vapor released from the melting sea ice.

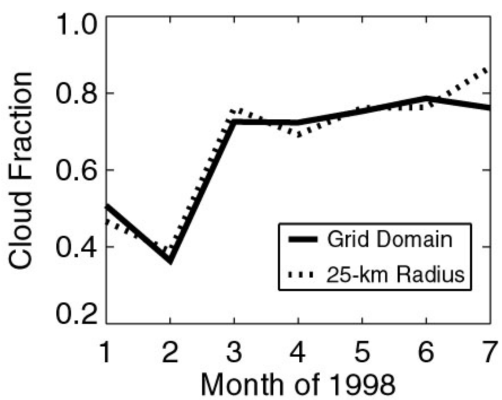

Figure 2. January-July 1998 cloud fraction observed for the SHEBA grid and 25-km radius.

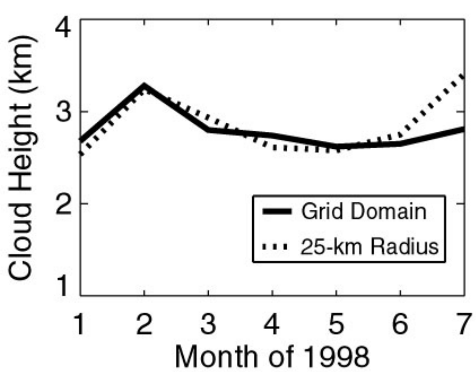

Figure 3. January-July 1998 cloud-top heights for the SHEBA grid and 25-km radius.

NOAA-AVHRR narrowband R_{06} albedos and T4 fluxes were converted into broadband shortwave (SW) and longwave (LW) fluxes using the empirical method of Doelling et al. (2001). Earth Radiation Budget Experiment (ERBE) and NOAA-9 AVHRR data from 1986 were matched to obtain the empirical regression fits. Cloud radiative forcing definitions at TOA for SW, LW, and net are respectively,

$$SWCRF = M_{SWCLR} - M_{SW} \tag{1}$$

$$LWCRF = M_{LWCLR} - M_{LW} \tag{2}$$

$$NETCRF = SWCRF + LWCRF \tag{3}$$

where M is the flux and the subscript CLR refers to clear-sky conditions. The monthly-hourly mean diurnal SW, LW, and net cloud forcing for the seasonal months of January, April, and July 1998 are shown in Fig. 4. SWCRF is 0 Wm^{-2} in January with values peaking at -60 Wm^{-2} in July when the surface is dark. SWCRF values are also larger for the greater incoming solar flux centered at 12 LT. April shows values down to -10 Wm^{-2}, indicating

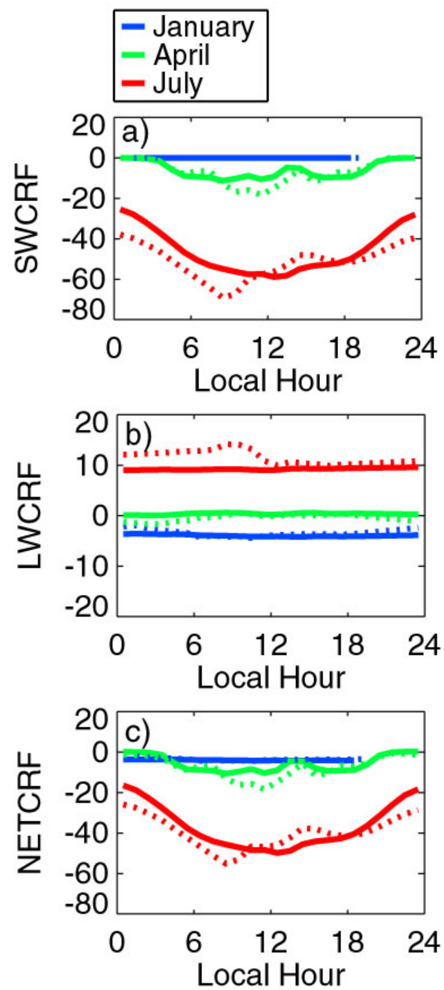

Figure 4. Diurnal TOA cloud radiative forcing for SHEBA. Solid lines are for the grid, dashed lines are for the 25-km radius.

the clouds were mostly brighter than the background snow surface. Positive LWCRF in Fig. 4b is most pronounced in July, with values around 10 Wm^{-2}. This indicates the presence of clouds mostly colder that the surface. Conversely, LWCRF is somewhat less than zero in January, indicating that clouds are mostly warmer than the cold snow surface. Because of the snow, ice, or ocean surface, minimal diurnal variability is seen in the LWCRF in Fig. 4b. In the LW, as winter changes to summer, clouds shift from having a cooling effect on the earth-atmosphere system to having a warming one. NETCRF in Fig. 4c is equal to LWCRF in January, with values around -3 Wm^{-2}. April shows a net loss of 0 to 10 Wm^{-2} of energy due to clouds over the course of a day. NETCRF values reach their minimum at 12 LT in July, with values at -50 Wm^{-2}. During all 3 seasons examined here, clouds acted to cool the earth-atmosphere system over the Arctic. The SHEBA cloud forcing values have the same trends as the regional grid with the greatest differences occurring in July.

The cloud amount, height, and cloud forcing distribution over the regional grid for January, April, and July 1998 is shown in Fig. 5. Large changes in cloud amounts of up to 50% can be seen in all 3 months across the grid, probably reflecting the strength of subsidence from Arctic high pressure in the cold season and the storm track in the melt season. The cloud amounts ranged from 30% in January over the northeast corner of the grid to 90% over northern areas in July. The cloud heights show the greatest change across the domain during July, with the storm track likely passing through the area of maximum cloudiness. A maximum in cloud height of 4 km occurs over the northern part of the grid in July near the SHEBA site. The net TOA cloud forcing shows little spatial variability in January and April with a 20+ Wm^{-2} change across the domain in July. This large spatial variability in NETCRF occurred because of the different surface conditions and cloud types existing over the domain in July. The cloud forcing values are between 0 and -10 Wm^{-2} in January and April with values commonly down to -40 Wm^{-2} in July.

6. CONCLUSIONS

An automated Arctic cloud mask was developed for NOAA-AVHRR to include day, night, and twilight viewing conditions. The daytime algorithm uses 3.7-μm reflectance models over snow while the nighttime and twilight algorithms are based on a brightness temperature threshold approach. The cloud mask captured most of the clouds seen in the radar and lidar, with rms errors between 18 and 32 percent. Cloud amounts significantly increased from winter to summer over the SHEBA site during 1998. The ship was located over an area of particularly high cloudiness in July compared to areas further south and east. Cloud heights over the western Arctic Ocean were nearly constant from winter to summer, with values around 2.7 km. Clouds caused the planet to cool during all seasons examined, with cooling from clouds most pronounced during the melt season. Over the seasons, the mean net cloud forcing ranged from -3 Wm^{-2} in winter to -50 Wm^{-2} in summertime at local noon.

The polar cloud mask will be run on the remaining months of the SHEBA year to include the late summer and autumn time periods. Temperature differences between the 11 and 12-μm channels may be used to detect thin cirrus clouds instead of Arctic haze for cases where the upper-level relative humidity is high. The cloud mask will be applied to data from more recent years over the ARM North Slope of Alaska site with new broadband fluxes derived from matched CERES broadband and TERRA-MODIS narrowband data.

REFERENCES

Doelling, D.R., P. Minnis, D.A. Spangenberg, V. Chakrapani, A. Mahesh, F.P.J. Valero, and S. Pope, 2001: Cloud radiative forcing at the top of the atmosphere during FIRE-ACE derived from AVHRR data. *J. Geophys. Res.*, **106**, 15,279-15,296.

Kratz, D.P., 1995: The correlated-k distribution technique as applied to the AVHRR channels. *J. Quant. Spectrosc. Radiative Transfer*, **53**, 501-517

Minnis, P., D.R. Doelling, V. Chakrapani, D.A. Spangenberg, L. Nguyen, R. Palikonda, T. Uttal, M. Shupe, and R.F. Arduini, 2001: Cloud coverage and height during FIRE-ACE derived from AVHRR data. *J. Geophys. Res.*, **106**, 15,215-15,232.

Simpson, J.J. and S.R. Yhann, 1994: Reduction of noise in AVHRR channel-3 Data with minimum distortion. *IEEE Trans. Geosc. and Remote Sens.*, **32**, 315-328.

Spangenberg, D.A., V. Chakrapani, D.R. Doelling, P. Minnis, and R.F. Arduini, 2001: Development of an automated arctic cloud mask using clear-sky satellite observations taken over the SHEBA and ARM-NSA sites.

Proc. AMS 6th Conf. On Polar Meteorology and Oceanography, San Diego, CA, May 14-18.

Spangenberg, D.A., D.R. Doelling, V. Chakrapani, P. Minnis, and T. Uttal, 2002: Nighttime cloud detection over the Arctic using AVHRR data. *Proc. 12th ARM Science Team Meeting*, St. Petersburg, FL, April 8-12.

Trepte, Q., R.F. Arduini, Y. Chen, S. Sun-Mack, P. Minnis, D.A. Spangenberg, and D.R. Doelling, 2001: Development of a daytime polar cloud mask using theoretical models of near-infrared bi-directional reflectance for ARM and CERES. *Proc. AMS 6th Conf. On Polar Meteorology and Oceanography*, San Diego, CA, May 14-18.

Young, D.F., P. Minnis, G.G. Gibson, D.R. Doelling, and T. Wong, 1998: Temporal interpolation methods for the Cloud's and the Earth's Radiant Energy System (CERES) Experiment. *J. Appl. Meteorol.*, **37**, 572-590.

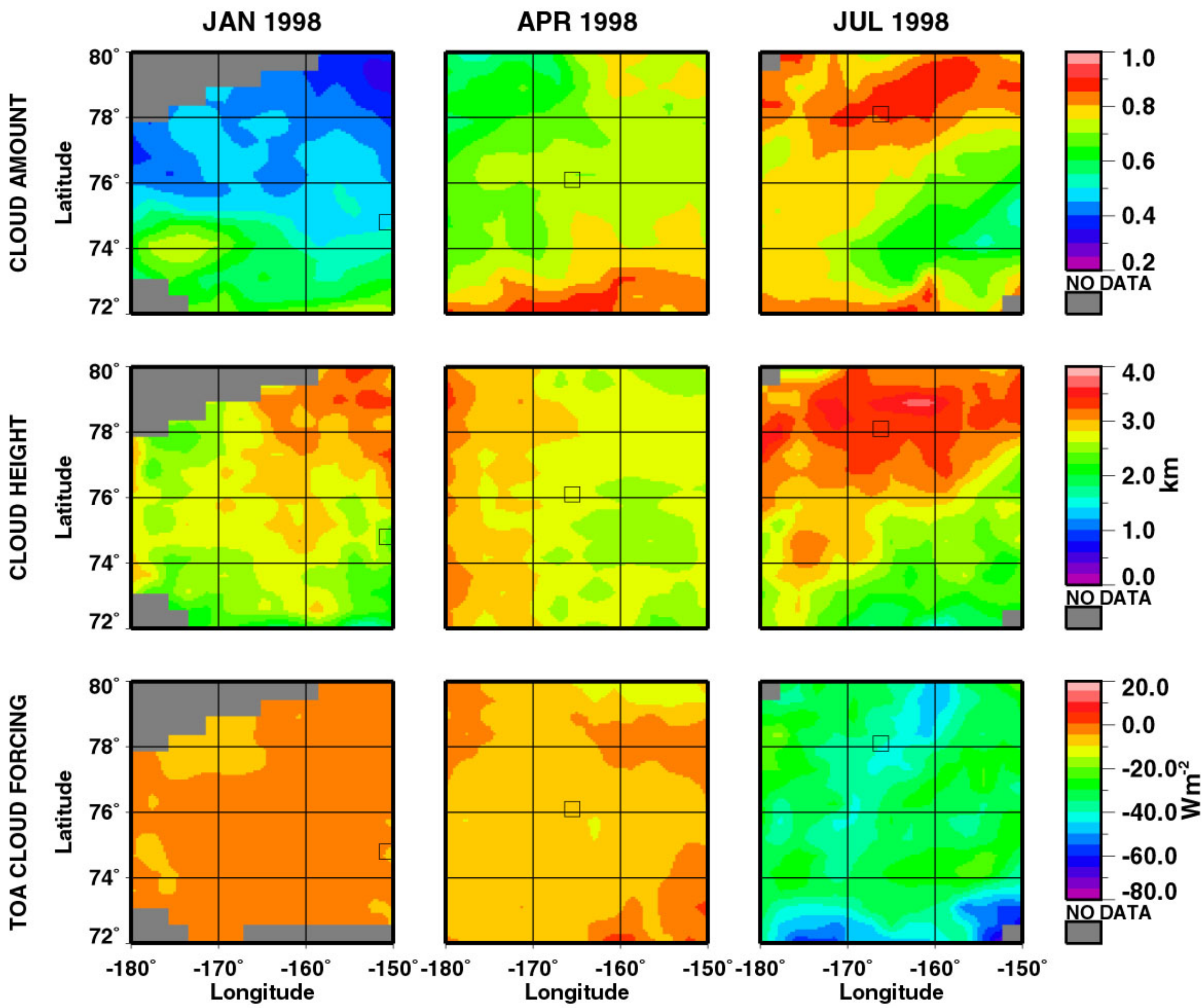

Figure 5. SHEBA cloud amounts, heights, and cloud radiative forcing on the regional grid for January, April, and July 1998.